# VERIFICATION OF THE OVERLAP RATIO INFLUENCE ON POWER AND MOMENT COEFFICIENTS OF A SAVONIUS WIND ROTOR USING COMPUTATIONAL FLUID DYNAMICS

**João Vicente Akwa, joaoakwa@gmail.com**
**Gilmar Alves da Silva Júnior, gilmar.alves@ufrgs.br**
**Adriane Prisco Petry, adrianep@mecanica.ufrgs.br**
Mechanical Engineering Department, Federal University of Rio Grande do Sul, Brazil

***Abstract.*** *This paper discusses the influence of the buckets overlap ratio of a Savonius wind rotor on the averaged moment and power coefficient, over complete cycles of operation. The equations of continuity, Reynolds Averaged Navier-Stokes – RANS and the Eddy Viscosity Model k-ω SST, in its Low-Reynolds approaches, with hybrid near wall treatment; are numerically solved using the commercial software Star-CCM+, based on Finite Volume Method, resulting in the fields of pressure and velocity of the flow and the forces acting on the rotor buckets. The moment and power coefficients are achieved through integration of forces coming from the effects of pressure and viscosity of the wind on the device. The influence of the buckets overlap ratio on the moment and power coefficients is checked by changing the geometry of the rotor, keeping the Reynolds number, based on rotor diameter, equal to 433,500. The results obtained for the rotor with zero overlap are in agreement with those obtained experimentally by other authors indicating that the method can be successfully used for such analysis. The values of the moment and power coefficients obtained as a function of tip speed ratio and the buckets overlap of the rotor indicates that the maximum device performance occurs for buckets overlap ratios with values close to 0.15.*

***Keywords****: Savonius wind rotor; buckets overlap ratio; CFD.*

## 1. INTRODUCTION

The use of unconventional devices like the Savonius wind rotor can be a solution for low cost and reduced environmental impacts for decentralized power generation. The wind rotor developed and patented in 1929 by Sigurd J. Savonius from Helsingfors at Finland, has, among other advantages: simple construction; high torque at startup and in full operation; accepting wind from any direction for the operation; low noise and low angular velocity in operation, which reduces wear on moving parts; in addition to various rotor configuration options, as for example, the use of multiple stages and different shapes of buckets (Savonius, 1930; Vance, 1973; Modi and Fernando, 1989). A Savonius wind rotor, however, cannot be regarded as a wind machine with performance higher and nor lower than performance of the other wind machines from power generation. Savonius rotors should only be understood as different mechanisms for the utilization of wind energy, and technological alternatives to conventional wind turbines (Vance, 1973; Eldridge, 1980). The device created by Savonius works mainly due to the resulting drag force on their buckets (Savonius, 1930). According to Akwa (2010), lift forces are also responsible for part of the power provided by the device.

As it was reported by Akwa (2010), the performance of a Savonius rotor is affected by flow parameters and geometry of the rotor. For a given flow configuration, different arrangements of Savonius rotor provide different performances in converting wind energy into useful energy. Studies about the influence of the buckets overlap ratio on the rotor performance are among the main research work carried out on such a device wind. In most previous studies on the influence of the buckets overlap ratio on the performance of Savonius rotor, it was reached the conclusion that a small overlap between the rotor buckets provides an improvement in the efficiency of the device. However, there is not yet an accurate indication of the optimum size of overlap in use; it reinforces the need for further investigation. According to Fujisawa (1992), the optimum size for the buckets overlap equals 15% of the size of the bucket chord. Blackwell *et al.* (1977) conclude that this dimension is equivalent to a value between 10 and 15% that size. Alexander and Holownia (1978) and Mojola (1985) indicate that values between 20 and 30% of the length chord provide the best results for the performance of Savonius wind turbines.

This paper discusses the influence of the buckets overlap ratio of a Savonius wind rotor on moment and power coefficients averaged over complete cycles of device operation. The results were obtained by applying the Finite Volume Method to solve the conservation equations of the turbulent air flow on the rotor, which allows the calculation of the performance coefficients of the rotor.

## 2. METHODOLOGY

### 2.1. Description of phenomenon

In this research work, the performance of a two bucket Savonius rotor with semicircular profiles buckets, like the one shown in Fig. 1, was analyzed. A two-dimensional modeling for the geometry of the rotor (Fig. 1-b) in operation is

performed, whereas in such a device, with high aspect ratio as can be seen in Figure 1-a, the changes in the profile of the flow caused by the effects of the bucket tips can be considered small. The operation of the rotor is simulated with variation in buckets overlap ratio ($R_s$). The buckets overlap ratio is obtained by the relationship between the overlap, $s$, and the chord, $c$, of the rotor buckets: $s/c$. In Figure 1-c, two-dimensional representations of the rotors tested with different buckets overlap ratios are displayed.

In Figure 1-b, the diameter of the end plate, $d_{pe}$, has a value of 1.1 m, while the value of the rotor diameter, $d_r$, is 1 m. The thickness of the buckets, $e$, is 4 mm and the spacing between the rotor buckets, $a$, is null. $\theta$ indicates the buckets angular position of the rotor that have a constant angular velocity, $\omega$, in wind with undisturbed velocity at a value equal to $V_o$. The parameters of the rotor and flow are always adjusted to each analysis keeping the Reynolds number, based on rotor diameter and undisturbed flow velocity, equal to 433,500.

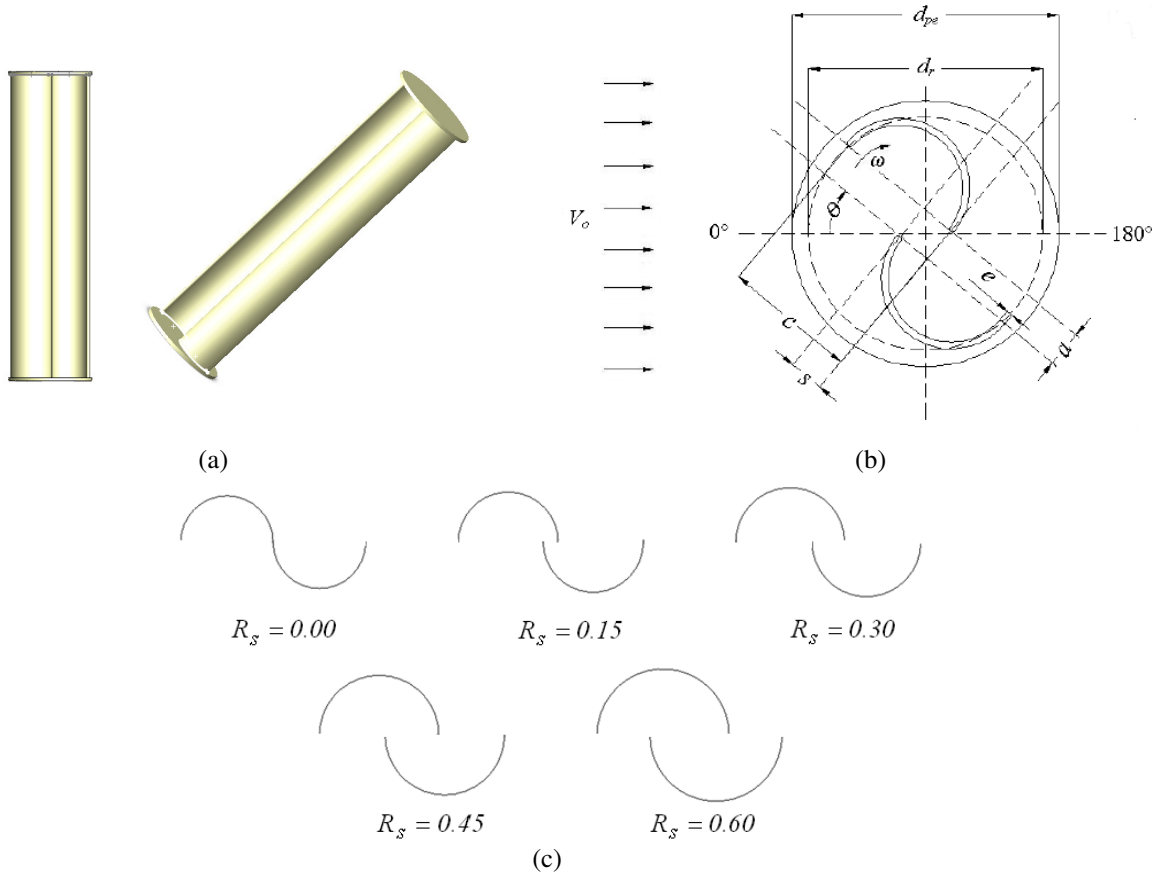


Figure 1. Savonius rotor: (a) 3D representation; (b) 2D representation; (c) geometry changes

The rotor is considered to be immersed in a turbulent air flow and operating at certain constant rotation rate. This phenomenon is reproduced by simulating the rotor operation in a domain that containing air under atmospheric conditions. The conservation equations of the turbulent air flow on the rotor are numerically solved for obtain the velocity and pressure fields in the calculation domain and the forces acting on the rotor buckets. The moment and power coefficients are achieved through integration of forces coming from the effects of pressure and viscosity of the wind on the device. The calculation domain is spatially discretized by cells of quad format to solve the equations using the Finite Volume Method (Patankar, 1980).

The dimensions of the calculation domain, given in multiples of the rotor diameter, and the boundary conditions adopted for the solution of conservation equations are shown in Fig. 2. The size of the calculation domain was chosen so that the boundaries just stay away from the rotor and thereby not affecting the performance of wind energy device, as is commented by Akwa (2010) and Silva Júnior (2010). Inside calculation domain, a circular region with mesh slide is bounded containing the contours of the rotor. This circular region has a diameter equivalent to 1.10 rotor diameters and center at 6 rotor diameters of the inlet and the sides of the calculation domain. At the inlet of the calculation domain, a velocity value for the air flow is prescribed, while at the outlet of the domain the pressure is considered equivalent to atmospheric pressure. The sides of the calculation domain are considered as symmetry planes. On the surface of the rotor, is considered the no-slip condition. As boundary conditions for calculating the effects of turbulence are used characteristic length and intensity of turbulence. As initial condition, it is considered homogeneous fields of pressure

and velocity in the flow. The rotation of the wind device is set to each simulation by specifying the rotation rate of the region of sliding mesh.

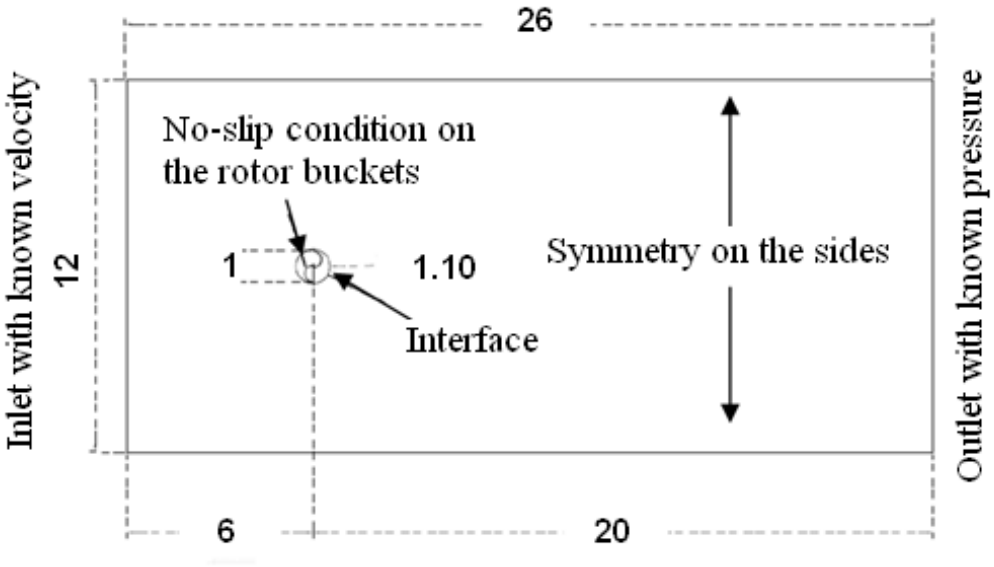


Figure 2. Calculation domain and boundary conditions

### 2.2. Details of the domain discretization

The equations of continuity, Reynolds Averaged Navier-Stokes – RANS and the Eddy Viscosity Model k-ω SST, in its Low-Reynolds approaches, with hybrid near wall treatment; are numerically solved using the commercial software Star-CCM+, based on Finite Volume Method, resulting in the fields of pressure and velocity of the flow and the forces acting on the rotor buckets. Applying this method, the calculation domain under study is divided into a finite number of elementary control volumes. The finite volume discretization transforms the differential equations governing the flow in a linear system of algebraic equations that is solved iteratively. This is due to the substitution of infinitesimal differences by finite differences in the differential equations. The calculated values of the variables are assigned to the centroids of each of the volumes. Thus the solution is discrete, depending on the number of elementary volumes present in the calculation domain (Maliska, 1995).

For purposes of domain discretization, a mesh with quadrilaterals volumes was done. The mesh consists by two parts: the first is fixed and the other is sliding (Fig. 3-a). The sliding mesh is located in the region circumscribed by the interface (Fig. 3-b). The sliding domain is constructed with a non-structured mesh, which ensures a better adaptation to the curved geometry of the rotor; while the fixed domain consists of a mapped mesh, ensuring a better organization and reducing the effects of numerical diffusion (Maliska, 1995; Akwa, 2010). Near the buckets are used layers of the finest volumes in order to improve the assessment of the boundary layer (Fig. 3-c).

### 2.3. Mathematical relationships and details of the used method

In this research work, the results were obtained by applying the Finite Volume Method to solve the conservation equations of the turbulent air flow on the rotor, which allows the calculation of the performance coefficients of the rotor. Among these conservation equations, there is a mass balance equation. The Equation (1) with indicial notation represents the mass balance where $\overline{u}_i$ is the average velocity of air flow and $u_i'$ is the velocity fluctuation due to the effects of turbulence, and $x$ represents the direction of flow. The momentum equation must be solved along with the mass balance equation. The Equation (2) represents the momentum equation, where $t$ is the time, $\overline{p}$ is average pressure, $\rho$ is the density and $\mu$ is the dynamic viscosity of atmospheric air.

$$\frac{\partial}{\partial x_i}\left(\overline{u}_i + u_i'\right) = 0 \tag{1}$$

$$\frac{\partial \overline{u}_i}{\partial t} + \overline{u}_j \frac{\partial \overline{u}_i}{\partial x_j} = -\frac{1}{\rho}\frac{\partial \overline{p}}{\partial x_i} + \frac{\mu}{\rho}\frac{\partial^2 \overline{u}_i}{\partial x_j \partial x_j} - \frac{\partial}{\partial x_j}\overline{u_i' u_j'} \tag{2}$$

From the Equation (2), arises the term $\rho\overline{u_i'u_j'}$ that is the stresses tensor of Reynolds introducing six additional unknowns. To solve the closure problem caused by the emergence of new unknowns, the turbulence model k-ω SST, in its Low-Reynolds approaches, is used because it's the one that best fits the studied phenomenon (Wilcox, 1998; Menter e Kuntz, 2002; Star-CCM+, 2008; Akwa, 2010). The model solves the equations of turbulent kinetic energy $k$, calculated by Eq. (3), and specific dissipation rate $\omega_t$, calculated by Eq. (4).

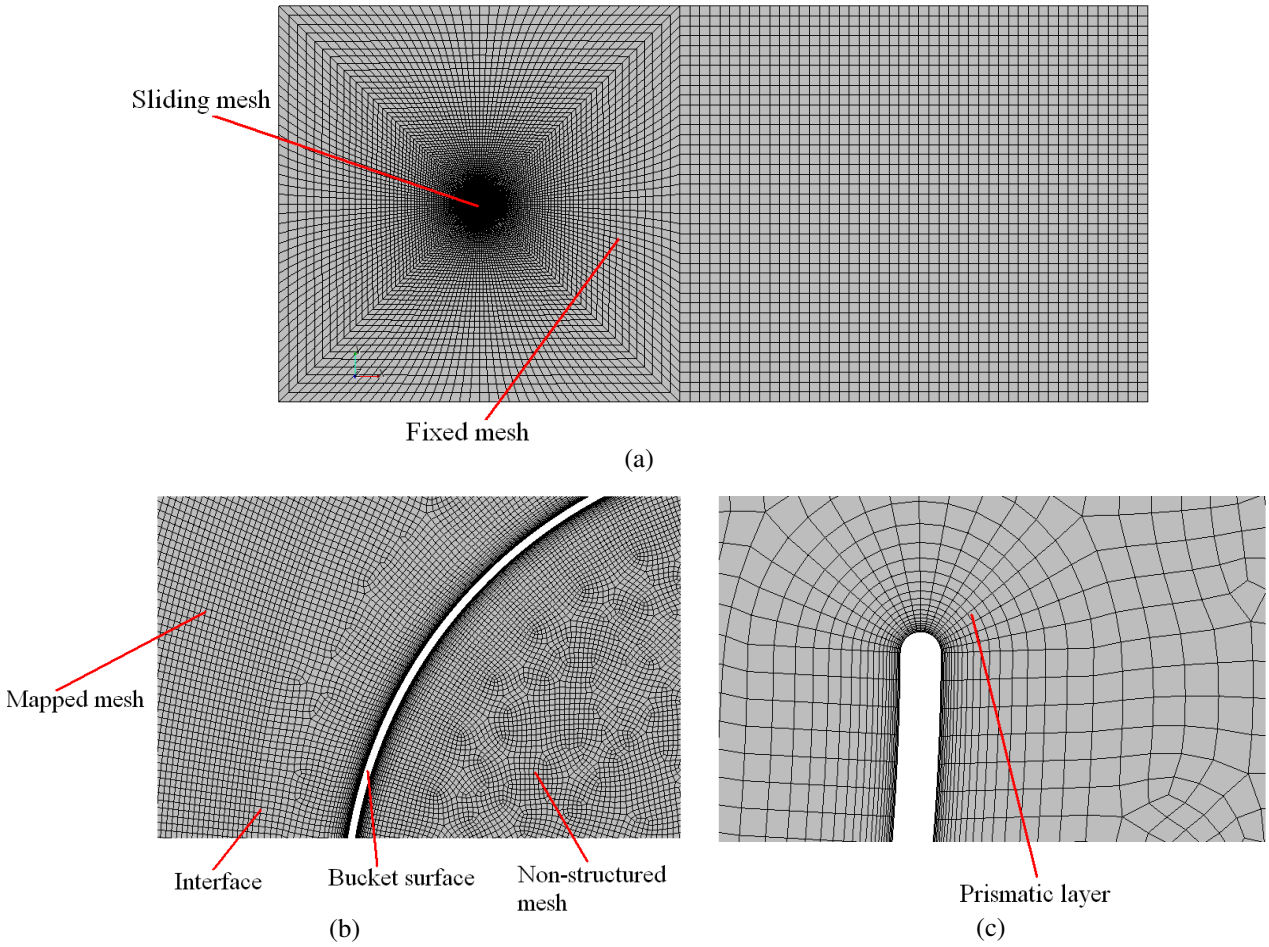


Figure 3. Used mesh: (a) overview of the discretizated domain; (b) region near the interface; (c) prismatic layer used

$$\frac{d}{dt}\int_V \rho k dV + \int_A \rho k\left(\boldsymbol{v}-\boldsymbol{v_g}\right)\cdot d\boldsymbol{a} = \int_A \left(\mu+\sigma_k\mu_t\right)\nabla k\cdot d\boldsymbol{a} + \int_V \left(\gamma_{eff}G_k - \gamma'\rho\beta^* f_\beta\left(\omega_t k-\omega_{t0}k_0\right)+S_k\right)dV \tag{3}$$

$$\frac{d}{dt}\int_V \rho\omega_t dV + \int_A \rho\omega_t\left(\boldsymbol{v}-\boldsymbol{v_g}\right)\cdot d\boldsymbol{a} = \int_A \left(\mu+\sigma_{\omega_t}\mu_t\right)\nabla\omega_t\cdot d\boldsymbol{a} + \int_V \left(G_{\omega_t} - \rho\beta f_\beta\left(\omega_t{}^2-\omega_{t0}^2\right)+D_{\omega_t}+S_{\omega_t}\right)dV \tag{4}$$

In the equations of turbulence model, $V$ is the cell volume, $A$ is area, $\boldsymbol{a}$ is a face area vector, $\boldsymbol{v}$ is velocity of the flow, $\boldsymbol{v_g}$ is the velocity of the grid, $\sigma_k$ and $\sigma_{\omega_t}$ are inverse turbulent Schmidt numbers, $\mu_t$ represents turbulent viscosity, $S_k$ and $S_{\omega_t}$ are the user-specified source terms, $k_0$ and $\omega_{t0}$ are the ambient turbulence values in source terms that counteract

turbulence decay, and $\gamma_{eff}$ is the effective intermittency provided by the Gamma ReTheta Transition model that is unity if this model is not activated. $\gamma'$ is calculated by Eq. (5).

$$\gamma' = min\left[max\left(\gamma_{eff}, 0.1\right), 1\right] \tag{5}$$

$G_{\omega_t}$ is the production of $\omega_t$ is evaluated by the Eq. (6), where $\gamma$ is a blended coefficient of the model and $S$ is the modulus of the mean strain rate tensor ($S = |\boldsymbol{S}|$). Similarly, the production of $k$, $G_k$, is defined by Eq. (7). $\boldsymbol{S}$ is evaluated by Eq. (8). $T_{k\omega_t}$ is a time scale that is computed using the Eq. (9).

$$G_{\omega_t} = \rho\gamma\left[\left(S^2 - \frac{2}{3}(\nabla\cdot\boldsymbol{v})^2\right) - \frac{2}{3}\omega_t\nabla\cdot\boldsymbol{v}\right] \tag{6}$$

$$G_k = \mu_t S^2 - \frac{2}{3}\rho k\nabla\cdot\boldsymbol{v} - \frac{2}{3}\mu_t(\nabla\cdot\boldsymbol{v})^2 \tag{7}$$

$$\boldsymbol{S} = \frac{1}{2}\left(\nabla\boldsymbol{v} + \nabla\boldsymbol{v}^T\right) \tag{8}$$

$$T_{k\omega_t} = min\left(\frac{1}{max\left(\omega_t/\alpha^*, (SF_2)/a_1\right)}, \frac{0.6}{\sqrt{3}S}\right) \tag{9}$$

The term $D_{\omega_t}$ in the Equation (4) is a cross-derivative term, defined by the Eq. (10).

$$D_{\omega_t} = 2(1-F_1)\rho\sigma_{\omega_t 2}\frac{1}{\omega_t}\nabla k\cdot\nabla\omega_t \tag{10}$$

The coefficients in the model are calculated from the blending function $F_1$, such that each coefficient $\phi$ is given by Eq. (11). The coefficients of Set 1 ($\phi_1$) are given by Eq. (12) and the coefficients of Set 2 ($\phi_2$) are given by Eq. (13). And in both Set 1 and Set 2 $\beta^*$ is 0.09 and $\alpha^*$ is 1.

$$\phi = F_1\phi_1 + (1-F_1)\phi_2 \tag{11}$$

$$\beta_1 = 0.0750\ ,\ \sigma_{k1} = 0.5\ ,\ \sigma_{\omega_t 1} = 0.5\ ,\ \kappa = 0.41\ ,\ \gamma_1 = \frac{\beta_1}{\beta^*} - \sigma_{\omega_t 1}\frac{\kappa^2}{\sqrt{\beta^*}} \tag{12}$$

$$\beta_2 = 0.0828\ ,\ \sigma_{k2} = 1.0\ ,\ \sigma_{\omega_t 2} = 0.856\ ,\ \kappa = 0.41\ ,\ \gamma_2 = \frac{\beta_2}{\beta^*} - \sigma_{\omega_t 2}\frac{\kappa^2}{\sqrt{\beta^*}} \tag{13}$$

The blending function $F_1$ is defined by Eq. (14), with $arg_1$ defined by the Eq. (15), where $y$ is the distance to the nearest wall, $CD_{k\omega_t}$ is related to the cross-diffusion term and $\nu$ is the kinematic viscosity $CD_{k\omega_t}$ is defined by Eq. (16).

$$F_1 = tanh\left(arg_1^4\right) \tag{14}$$

$$arg_1 = min\left(max\left(\frac{\sqrt{k}}{0.09\omega_t y}, \frac{500\nu}{y^2\omega_t}\right), \frac{2k}{y^2 CD_{k\omega_t}}\right) \tag{15}$$

$$CD_{k\omega_t} = max\left(\frac{1}{\omega_t}\nabla k \cdot \nabla \omega_t, 10^{-20}\right) \tag{16}$$

The Equation (17) expresses the function $F_2$, where the coefficient $a_1$ is equal to 0.31 and $arg_2$ is given by the Eq. (18).

$$F_2 = tanh\left(arg_2^2\right) \tag{17}$$

$$arg_2 = max\left(\frac{2\sqrt{k}}{0.09\omega_t y}, \frac{500\nu}{y\omega_t}\right) \tag{18}$$

The relations to find the turbulent viscosity are obtained through the solution of Eq. (3) and (4). Thus, the turbulent viscosity $\mu_t$ can be expressed by Eq. (19) and related to the Reynolds tensor by Eq. (20), solving the closure problem. In the Equation (20), $\delta_{ij}$ is the Kronecker delta operator.

$$\mu_t = \rho k T_{k\omega_t} \tag{19}$$

$$-\rho\overline{u_i' u_j'} = \mu_t\left(\frac{\partial \overline{u}_i}{\partial x_j} + \frac{\partial \overline{u}_j}{\partial x_i}\right) - \frac{2}{3}\rho k \delta_{ij} \tag{20}$$

A hybrid treatment solution on the wall was done in this research work. Using this treatment, the laminar sub layer in the region of fine mesh, for dimensionless wall distance, $y^+$, less than three, is calculated and in other areas it use a logarithmic profile for the boundary layer. $y^+$ is evaluated by the Eq. (21), where $u^*$ is a reference velocity. For the hybrid wall treatment, or all $y^+$ wall treatment, that is used in this work, a hybrid function $g$ is defined in terms of Reynolds number based on distance from the wall, $Re_y$, according to Eq. (22).

$$y^+ = \frac{y u^* \mu}{\rho} \tag{21}$$

$$g = exp\left(\frac{Re_y}{11}\right) = exp\left(\frac{\sqrt{ky/v}}{11}\right) \tag{22}$$

The reference velocity $u^*$, production in the wall cell $G_k$ and specific dissipation in the wall cell $\omega_t$, are given by Eq. (23), (24) and (25), respectively, where $u^+$ is wall-parallel velocity ($u$) non-dimensionalized with $u^*$.

$$u^* = \sqrt{\frac{g\nu u}{y} + (1-g)\beta^{*1/2} k} \tag{23}$$

$$G_k = g\mu_t S^2 + \frac{(1-g)}{\mu}\left(\frac{\rho u^* u}{u^+}\right)^2 \frac{\partial u^+}{\partial y^+} k \tag{24}$$

$$\omega_t = g\frac{6\nu}{\beta y^2} + (1+g)\frac{u^*}{\sqrt{\beta^*}\kappa y} \tag{25}$$

The boundary condition for $k$ on the walls is $\partial k/\partial n\big|_w = 0$, with $n$ indicating the normal direction, and for $\omega_t$ is specified in the wall cells according to the appropriate method in the wall treatment. The Equations (26) and (27) are

used as initial conditions for $k$ and $\omega_t$, respectively, where $I$ is turbulence intensity and $L$ is length scale. In this research work, it was assumed the turbulence intensity equal to 1% and the length scale of 0.01 m at the calculation domain. These values are used in the rest of the calculation domain as an initial condition. $\beta^+$ is a coefficient of the model.

All these equations are discretized through the Finite Volume Method, which creates a system of linear algebraic equations that is solved iteratively using the Gauss-Seidel Method. The temporal terms of the equations are discretized using a fully implicit temporal scheme of 2nd order. The discretization of the advective terms of the conservation equations, responsible for the transport of scalar variables through the motion of fluid particles in the flow, is achieved by the interpolation function Second Order Upwind, more accurate than first order schemes. The method SIMPLE (Semi Implicit Linked Equations) is used to make the coupling between pressure and velocity calculations, ensuring good stability for the solution (Maliska, 1995; Star-CCM+, 2008; Akwa, 2010; Silva Júnior, 2010).

Holding the solution of conservation equations and turbulence model, one can obtain the rotor moment, $T$, by integrating the forces resulting from the tensions that act on the buckets. The rotor moment is calculated by Eq. (28), where $\boldsymbol{F}_f^{\boldsymbol{pressure}}$ and $\boldsymbol{F}_f^{\boldsymbol{shear}}$ are the pressure and shear force vectors and $\boldsymbol{d}$ is a vector defining the axis through point $\boldsymbol{x_0}$ about which the moment is taken and $\boldsymbol{k}_f$ is the position of face $f$ relative to $\boldsymbol{x_0}$. The pressure force vector on surface face $f$ is computed from: $p_f$ that is the face pressure, $\boldsymbol{d}_f$ that is the face area vector, and $p_{ref}$ that is the reference pressure. As defined, this is the force that the fluid exerts on the surface. The shear force on surface face $f$ is computed by the stress tensor at face $f$, $\boldsymbol{\tau}_f$, and $\boldsymbol{d}_f$. This is the shear force exerted on the surface by the fluid (Star-CCM+, 2008).

$$k \approx \frac{3}{2}(Iv)^2 \tag{26}$$

$$\omega_t \approx \frac{\sqrt{k}}{L\beta^{+1/4}} \tag{27}$$

$$T = \sum_f \left[\boldsymbol{k}_f \times \left(\boldsymbol{F}_f^{\boldsymbol{pressure}} + \boldsymbol{F}_f^{\boldsymbol{shear}}\right) \cdot \boldsymbol{d}\right] = \sum_f \left\{\boldsymbol{k}_f \times \left[\left(p_f - p_{ref}\right)\boldsymbol{d}_f + \left(-\boldsymbol{\tau}_f \cdot \boldsymbol{d}_f\right)\right] \cdot \boldsymbol{d}\right\} \tag{28}$$

With the moment value obtained by Eq. (28) and the value of the rotation rate, $\omega$, which is imposed as a boundary condition in each simulation, the rotor power, $P$, can be calculated because $P = T\omega$. Dividing the rotor power by the power available in the air flow that focuses on the projected area of the rotor, $A_r$, one can obtain the relationship between the power coefficient, $C_P$, moment coefficient, $C_T$, and the tip speed ratio of the rotor, $\lambda$. This relationship, which is used to calculate the dimensionless aerodynamics coefficients of the rotor, is represented by the Eq. (29), where $r$ is the radius of the Savonius rotor. The results of this research work are expressed by the averaged moment and power coefficients as functions of tip speed ratio of the rotor for a Reynolds number equal to 433,500 (Akwa, 2010).

$$C_P = \frac{P}{P_{available}} = \frac{T\omega}{1/2\,\rho\, A_r V_o^3} = \frac{T}{1/2\,\rho\, A_r V_o^2}\,\frac{r\omega}{r}\,\frac{r}{V_o} = C_T\lambda \tag{29}$$

As the methodology adopted by Silva Júnior (2010), the value of time step, $\Delta t$, used in the discretization of conservation equations, is related to the smaller size of the smallest cell in the discretized calculation domain, $\Delta x_{min}$, by Eq. (30), where $r_{int}$ is the radius of the area enclosed by the boundary condition interface. For this equation, the space discretization is done coupled with the temporal discretization, ensuring Courant number of unit in all simulations (Star-CCM +, 2008).

$$\Delta t = min\left(\frac{\Delta x_{min}\, r}{r_{int}\,\lambda\, V_o}, \frac{\Delta x_{min}}{V_o}\right) \tag{30}$$

The flow conservation equations are then discretized and solved by Finite Volume Method, obtaining the necessary values for calculating the aerodynamics coefficients of the rotor. Simulations were performed to verify that the values of aerodynamic coefficients obtained by the method were independent of the level of discretization, using the rotor with $R_s = 0$ and $\lambda = 1$, for meshes containing 39,889 and 329,869 cells. Using 329,869 cells to discretize the calculation domain, the averaged power coefficient differs only 2.26% of the value obtained with the use of 39,889 cells. Given the right combination of accuracy and computational effort, the space discretization in the other simulations were done in order to provide the average size of the cells of the order of 0.09 m to a value of about 0.0007 m for the value of $\Delta x_{min}$. A computer simulation was also performed to a value of time step equal to half the value obtained by Eq. (30). This

simulation resulted in a value of averaged power coefficient that differs in 0.027% of the previous equivalent value, indicating that the use of the Eq. (30) provides satisfactory results.

## 3. RESULTS AND DISCUSSION

Pressure and velocity fields similar to those shown in Fig. 4 for the air flow over the rotor are obtained by solving the conservation equations of the flow by Finite Volume Method. In Figure 4, the complex flow of air over the Savonius rotor can be observed. In this figure, the pressure differences on the buckets, which generate pressure drag, the main strength related to the operation of this type of wind turbine can also be observed. Such fields obtained allow several qualitative analysis of the flow.

The integration of the forces on the rotor buckets allows obtaining quantitative data of moment and power coefficients, which allow comparison with other studies. In Figure 5, the values of averaged power coefficients, which were obtained by simulation with Savonius wind rotor without buckets overlap and operating at different tip speed ratios (dimensionless rotation rate), can be observed. From Figure 5, it appears that the results are representative of the analyzed phenomenon because the simulated values are in agreement with those measured by Blackwell *et al.* (1977) for similar rotor and flow conditions.

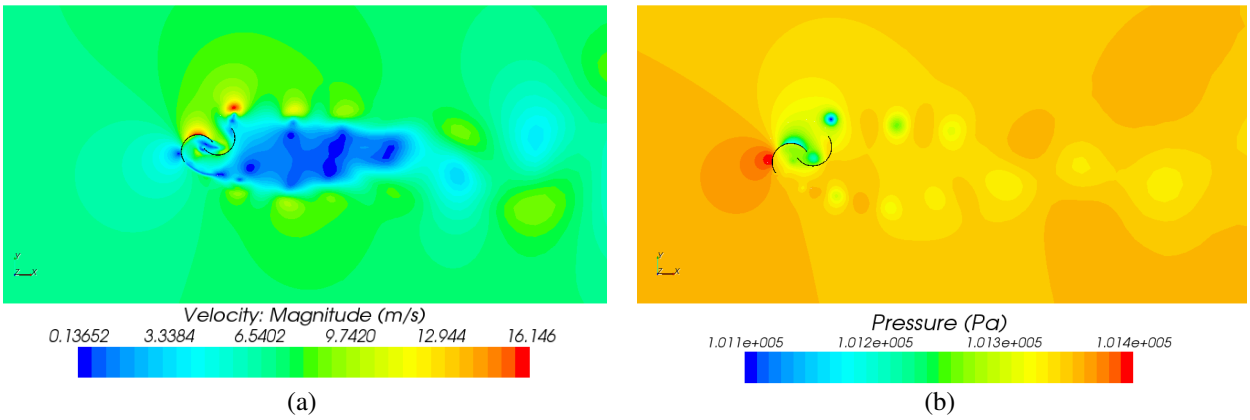


Figure 4. Fields of the air flow for $R_s = 0.30$ and $\lambda = 1.25$: (a) velocity; (b) pressure

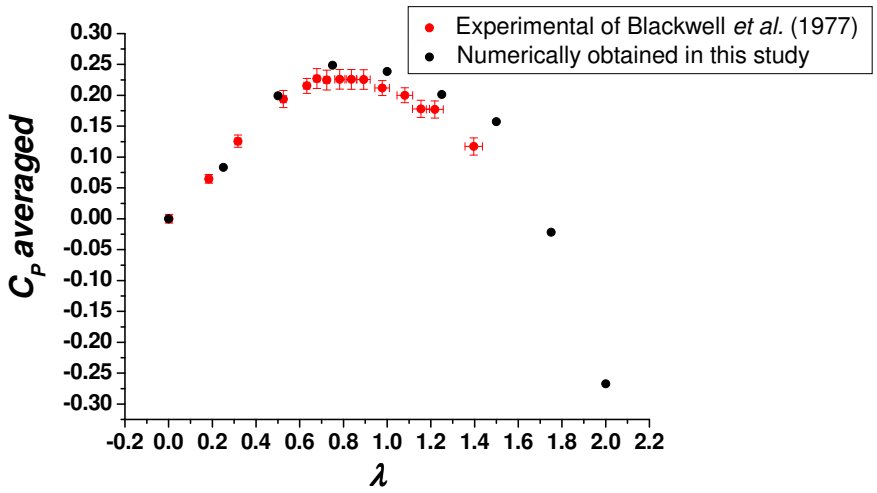


Figure 5. Averaged power coefficient *versus* tip speed ratio for $R_s = 0.00$

In the Figures 6 and 7, the obtained values for the averaged moment and power coefficients for other buckets overlap ratios are shown. Through these figures, it can be observe that the rotor has a better performance for $R_s$ values of 0.15, with averaged power coefficient equal to 0.3161 for the tip speed ratio equal to 1.25. One can also observe that the high starting moment (for low values of $\lambda$) of a Savonius wind rotor increases as the values of $R_s$ grow to a certain value from which the moment and performance of the rotor fall dramatically due to the decreased incidence of air on the concave side of the rotor buckets.

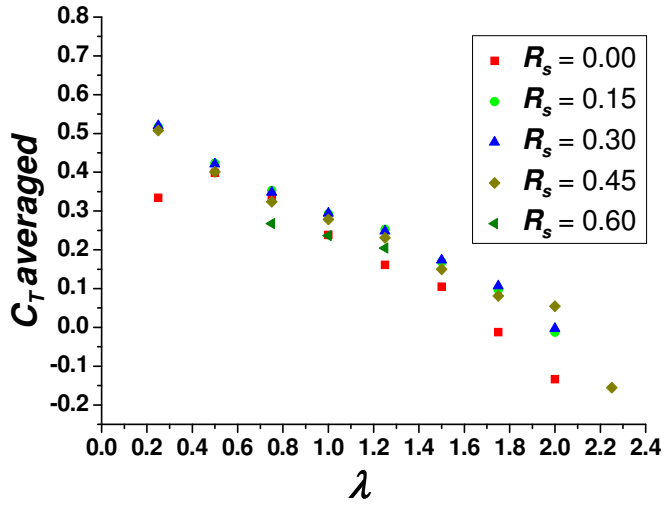


Figure 6. Averaged moment coefficient *versus* tip speed ratio

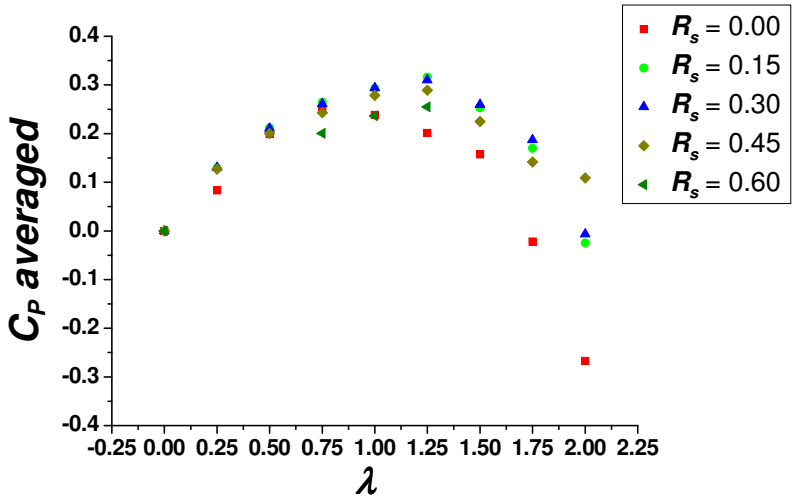


Figure 7. Averaged power coefficient *versus* tip speed ratio

In Figure 8, the velocity vectors for the condition of better rotor performance are displayed. The air flow between the rotor buckets which increases pressure on the concave side of returning bucket and improves performance does not occur satisfactorily for low values of $R_s$. Recirculations that promote loss of momentum occur for extreme values of $R_s$.

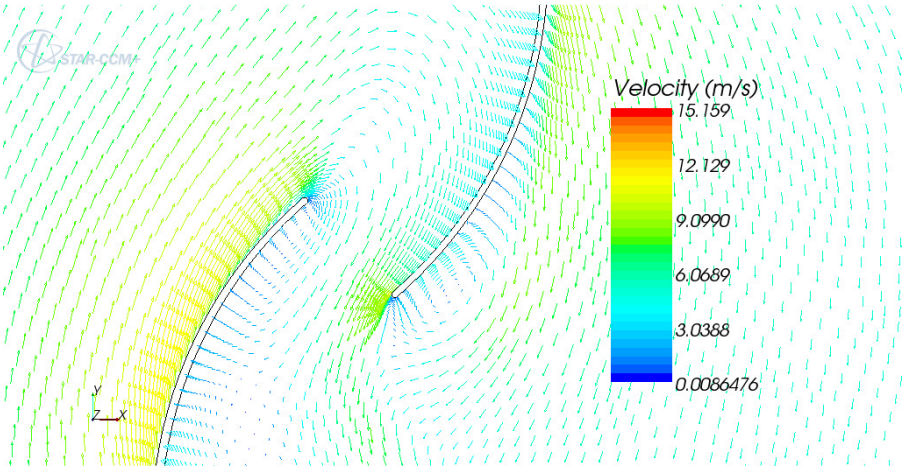


Figure 8. Velocity vectors for Savonius rotor operating at $R_s$ = 0.15 and $\lambda$ = 1.25

## 4. CONCLUSIONS

This study is developed in order to verify numerically the influence of different buckets overlap ratios in the performance of Savonius wind turbines, with the aim of optimizing the geometry of the wind device. This research work gets physically consistent results and has good agreement with another study. Thus, one can conclude that the used parameters are suitable for this analysis. The obtained pressure and velocity fields are as expected. The configuration that shown best performance is the one for which $R_s = 0.15$, which gives an averaged power coefficient equal to 0.3161 for the tip speed ratio equal to 1.25. The use of buckets overlap creates spacing between the rotor buckets, allowing the passage of air from the advancing bucket for the returning bucket. This leads to an increase of moment in this rotor type to a limit value. This increase in the rotor performance occurs because the air flows from the advancing bucket for the returning bucket increasing pressure on the concave side of the returning bucket and reducing the drag force on this rotor part. However, for high buckets overlap, the moment and performance of the rotor fall dramatically due to the decreased incidence of air on the concave side of the rotor buckets.

In future researches, new settings for wind rotors can be analyzed so it can get an optimized model. It is interesting also perform 3D simulations of rotor to the 3D parameters that affect performance, such as aspect ratio, can be analyzed. Moreover, effects of the terrain, turbulence intensity and shaft can be included in the simulations to provide more realistic conditions.

This study confirms that the Finite Volume Method can be applied successfully to the study of Savonius turbines. The explained methodology is a promising tool, since it helps to steer future improvements of this rotor, optimizing their performance.

## 5. ACKNOWLEDGEMENTS

The authors thank the financial support from CNPq through scholarship grant to Akwa, J. V.

## 6. REFERENCES

Akwa, J. V., 2010, "Análise Aerodinâmica de Turbinas Eólicas Savonius Empregando Dinâmica dos Fluidos Computacional", Federal University of Rio Grande do Sul, Porto Alegre, Brazil, 128 p.

Alexander, A. J., Holownia, B. P., 1978. "Wind Tunnel Tests on a Savonius Rotor". Journal of Industrial Aerodynamics, Vol. 3, No. 4, pp. 343-351.

Blackwell, B. F., Sheldahl, R. E., Feltz, L. V., 1977, "Wind Tunnel Performance Data for Two- and Three-Bucket Savonius Rotors", Final Report SAND76-0131, Sandia Laboratories, Albuquerque, USA, 105 p.

Eldridge, F. R., 1980, "Wind Machines", Ed. Van Nostrand Reinhold Company, New York, USA, 214 p.

Fernando, M. S. U. K., Modi, V. J., 1989. "A Numerical Analysis of the Unsteady Flow Past a Savonius Wind Turbine". Journal of Wind Engineering and Industrial Aerodynamics, Vol. 32, pp. 303-327.

Fujisawa, N., 1992. "On the Torque Mechanism of Savonius Rotors". Journal of Wind Engineering and Industrial Aerodynamics, Vol. 40, No. 3, pp. 277-292.

Maliska, C. R., 1995, "Transferência de Calor e Mecânica dos Fluidos Computacional", Ed. LTC, Rio de Janeiro, Brazil, 1995.

Menter, F. R., Kuntz, M., 2002, "Adaptation of Eddy Viscosity Turbulence Models to Unsteady Separated Flows Behind Vehicles", In: The Aerodynamics of Heavy Vehicles: Trucks, Buses and Trains, Ed. Springer, Asilomar, CA.

Mojola, O. O., 1985. "On The Aerodynamic Design of The Savonius Windmill Rotor". Journal of Wind Engineering and Industrial Aerodynamics, Vol. 21, pp. 223-231.

Patankar, S.V., 1980, "Numerical Heat Transfer and Fluid Flow", Ed. McGraw-Hill, New York, USA.

Savonius, S. J., 1930, "Wind Rotor – Patent 1,766,765", United States Patent Office.

Silva Júnior, G. A., 2010, "Análise da Influência de Diferentes Razões de Sobreposição no Desempenho de Turbinas Eólicas Savonius Empregando Dinâmica dos Fluidos Computacional", Federal University of Rio Grande do Sul, Porto Alegre, Brazil, 21 p.

Star-CCM+, 2008, "Methodology", CD-adapco.

Vance, W., 1973, "Vertical Axis Wind Rotors – Status and Potential", Proceedings of the Conference on Wind Energy Conversion Systems, Vol.1, Washington, USA, pp. 96-102.

Wilcox, D.C., 1998, "Turbulence Modeling for CFD", DCW Industries, Inc., 1998.

## 7. RESPONSIBILITY NOTICE

The authors are the only responsible for the printed material included in this paper.